

Article

Isotherms, Kinetics, and Thermodynamics of NH_4^+ Adsorption in Raw Liquid Manure by Using Natural Chabazite Zeolite-Rich Tuff

Giulio Galamini, Giacomo Ferretti , Valeria Medoro , Nicola Tescaro, Barbara Faccini  and Massimo Coltorti

Department of Physics and Earth Science, University of Ferrara, via Saragat 1, 44122 Ferrara, Italy; glmgli@unife.it (G.G.); mdrvlr@unife.it (V.M.); nicola.tescaro@student.unife.it (N.T.); fcbbr@unife.it (B.F.); clt@unife.it (M.C.)

* Correspondence: frrgcm@unife.it

Received: 2 October 2020; Accepted: 19 October 2020; Published: 21 October 2020



Abstract: The search for safer and sustainable management of animal manure is a global and topical challenge, in particular for the reduction of nitrogen (N) content. The use of natural adsorbents as zeolite-rich tuffs is recognized as a valid method to recover N, in the form of ammonium (NH_4^+), from animal manure. While the scientific literature is rich in studies performed on synthetic solutions and using clinoptilolite zeolites as adsorbent, it lacks information concerning adsorption in real liquid manure and using other types of zeolite-rich tuffs (e.g., chabazite). This work aims at exploring the NH_4^+ adsorption process from raw liquid swine manure, using a chabazite-rich zeolite tuff as adsorbent. The effects of temperature, contact time, and grain size have been assessed. Isotherms, kinetic models, and thermodynamic parameters have been investigated. Harkins-Jura isotherm correlates well with the observed data, in accordance with the formation of an adsorption multilayer. Kinetic data have been explained by intraparticle diffusion and pseudo-second-order models. In conclusion, the natural chabazite tuff has proven to be a valid material for NH_4^+ adsorption from raw liquid swine manure. In particular, to reach the highest adsorption capacities and adsorption rates, it is recommended to use it at a fine particle size and with dosages $< 6\%$.

Keywords: wastewater treatment; livestock; natural zeolite; sustainable agriculture; environmental pollution; nitrogen removal

1. Introduction

The intensification of agricultural activities to meet the increasing demand for food and agricultural products is leading to rapid soil degradation and severe environmental problems like GHG emissions and water pollution. The Food and Agriculture Organization of the United Nations (FAO) has declared that “to satisfy the expected food and feed demand, it will require a substantial increase of global food production of 70 percent by 2050, involving an additional quantity of nearly 1 billion tons of cereals and 200 million tons of meat” [1]. Intensive farming brings huge quantities of chemical and organic fertilizers in the soil every year to improve productivity, but this massive amount of nutrients are inefficiently exploited by plants and they are largely lost in the environment [2,3]. The need to improve fertilizer use efficiency (FUE) thus represents one of the major challenges for the upcoming years and it is essential for achieving more sustainable agriculture.

Another global challenge that we are forced to face in the immediate future is the increasing demand for meat, which is rising according to the economic growth of countries like South America, India, and China. As a direct consequence of increased meat demand, large amounts of zootechnical

wastewaters rich in nitrogen (N) and phosphorous (P) are produced every year and often used as organic fertilizer, with a strong impact on climate and environment [4–6]. The environmental pollution resulting from the release of large quantities of nutrients in the soil, water, and atmospheric compartments is generically termed “nutrient pollution”. It affects the quality of soil, underground and surface waters, their ecosystems, the climate (due to the emissions of N-based GHG and harmful gases such as N_2O , NH_3 , and NO_x), the human health, and the economy [7–9].

It is thus mandatory to develop proper management practices that aim at reducing the nutrient load of zootechnical wastewaters before application in the soil to improve the FUE and reduce nutrient pollution.

A valid methodology for the reduction and recycling of N consists of the so-called “Integrated Zeolite Cycle” (IZC). The IZC promotes the use of natural materials as zeolite-rich tuffs (ZRT) in agricultural contexts, as agent for the removal of ammonium ions (NH_4^+) dissolved in animal liquid manure, and their subsequent use as soil amendments [10–12]. ZRT are volcanic rocks containing more than 50% of zeolite minerals [13]. Zeolites are aluminosilicate minerals with an open 3D-structure formed by linked tetrahedra of $[\text{SiO}_4]^{4-}$ and $[\text{AlO}_4]^{5-}$, which constitute their primary building units. The replacement of Si^{4+} by Al^{3+} induces a negative charge in the zeolite framework, which is compensated by the presence of extra-framework cations (counterions). These cations can be exchanged by other cationic species present in the surrounding aqueous solution [14,15]. This process, called ion-exchange, is mainly governed by charge neutrality and by diffusion dynamics [16]. In addition to cations, large quantities of water molecules surrounding these ions (so-called hydration spheres) can also enter the pore structure, allowing zeolites great hydration and dehydration capacity. Many studies published in recent years have shown how the application of ZRT in the soil brings important positive effects like the increase of FUE and the reduction of gaseous and leaching N losses [17–21].

Within natural zeolites, clinoptilolite is one of the most abundant and studied and, thanks to its adsorption and ion exchange properties, it finds application in numerous contexts such as water and wastewater treatment, agriculture [22], and the medical field [23]. Another important type of zeolite, however abundant and distributed throughout the world, is chabasite, which is not yet sufficiently studied and used, although it represents a valid alternative to the better-known clinoptilolite. Due to its high cation exchange capacity (CEC), chabasite has an excellent potential for applications like water and wastewater treatment, even greater than clinoptilolite (theoretical CEC of clinoptilolites varies between 2.0 and 2.6 meq gram^{-1} , while CEC of chabazite is generally between 2.5 and 4.7 meq gram^{-1} [24]).

Moreover, while adsorption of NH_4^+ has been largely investigated in synthetic solutions (especially $(\text{NH}_4)_2\text{CO}_3$ and NH_4Cl) [25–32] and, to a limited extent, also in anaerobic digestates (using NaCl-modified clinoptilolite) [33], as of today there are no studies that provide a detailed characterization of NH_4^+ adsorption (isotherms, kinetics, and thermodynamics) in real animal liquid manure by using chabazite ZRT.

Wasielowski et al. [26] proposed a possible guideline for the determination of NH_4^+ adsorption processes from high concentrated wastewaters by clinoptilolite ZRT. In this paper, we present a series of experiments in which we followed a similar protocol to characterize the isotherms, kinetics, and thermodynamics of NH_4^+ adsorption using a chabazite ZRT in real animal liquid manure.

The experiments included the evaluation of temperature, contact time, and particle size effects.

2. Materials and Methods

2.1. Materials

The chabazite ZRT used in this experiment was quarried near Sorano village (Italy, $42^\circ 41' 26.53''$ N; $11^\circ 44' 35.07''$ E) and supplied by Verdi S.p.a. company. Its chemical-physical and mineralogical characteristics are indicated by Malferrari et al. [34]; briefly chabazite 68.5%, k-feldspar 9.7%, mica 5.3%, pyroxene 2.9%, phillipsite 1.8%, analcime 0.6%, volcanic glass 11.2%. Its CEC is 2.17 meq g^{-1} ;

exchangeable bases naturally contained in the tuff are Ca^{2+} 1.46, K^{+} 0.60, Na^{+} 0.07 and Mg^{2+} 0.04 meq g^{-1} .

Two particle sizes were selected for the experiments, a granular one (CHAg) and a micro-sized one (CHA μ). The particle size distribution of CHAg has been previously characterized using the sequential sieving method (12.5% between 5 and 2 mm, 60.4% between 2 and 0.8 mm, 24.1% between 0.8 and 0.425 mm, and 3% less than 0.425 mm). CHA μ particle size has been characterized using a sedigraph (Micromeritics 5100). The results are expressed following the Wentworth classification (1922): 0.4% between 250 and 125 μm (fine sand), 2.8% between 125 and 62.5 μm (very fine sand), 75.6% between 62.5 and 3.9 μm (silt), and 21.2% less than 3.9 μm (clay).

Both CHA μ and CHAg were dried at 105 °C for 24 h to eliminate the gravimetric water before the beginning of the experiments.

Liquid pig manure was obtained from a pig farm located near Rovigo (Italy). Immediately after sampling, the liquid manure was centrifuged at 4000 rpm for 8 min to eliminate the coarser fraction. The supernatant was collected to obtain the liquid phase to be tested in the experiments (centrifuged swine manure, CSM). Initial CSM pH and $[\text{NH}_4^+]$ were 8.07 ± 0.03 and $3140 \pm 45 \text{ mg L}^{-1}$, respectively (measured in 4 replicates; see Section 2.2 for analytical techniques used).

2.2. Analytical Techniques

$[\text{NH}_4^+]$ was measured in a dilution ratio of 1:20 CSM/Milli-Q water, using an Ion-Selective Electrode (ISE) Orion 95–12. Solution pH was measured using an Orion 9102BNWP pH-meter. Both ISE and the pH-meter were connected to an Orion 4star pH–ISE benchtop (Thermo Fisher Scientific, Waltham, MA, USA).

2.3. Experimental Design

2.3.1. Isotherms

Equilibrium experiments aimed at evaluating the Isotherm models for CHA μ and CHAg at three different temperatures (13, 20, and 37 °C).

Different quantities of CHA (0.5, 1, 1.5, 3, 5, 8, and 12 g) were mixed with 50 mL of CSM inside closed plastic bottles (50 mL) in three replicates and stirred with an orbital shaker at 200 rpm for 20 h to reach the equilibrium condition. Many studies have reported that NH_4^+ sorption by zeolites is affected by pH without significant differences in the range 2–8 and with an immediate decrease at $\text{pH} > 9$ [35,36]. In real conditions it is preferable not to control the pH using chemical buffers added to the wastewater and, since pH barely varied between 8.07 and 8.48 from the beginning of the experiment to the equilibrium conditions, we decided to neglect the pH effects and not to buffer the CSM. The possible air stripping effects and/or adsorption onto plastic parts of the bottles were taken into account in the experiments, providing blanks with only CSM and without the addition of zeolite. After 20 h of shaking, the samples (CSM + CHA and blanks) were centrifuged at 4000 rpm for 8 min to separate the solid phase from the liquid. NH_4^+ equilibrium adsorption capacity (q_e , mg g^{-1}) was determined in the supernatant by Equation (1) [26]:

$$q_e = \frac{(C_0 - (C_0 - C_b) - C_e) \times V}{m} \quad (1)$$

where C_0 (mg L^{-1}) is the initial NH_4^+ concentration, C_b (mg L^{-1}) is the NH_4^+ concentration in blanks after 20 h, C_e (mg L^{-1}) is the concentration at equilibrium, V (L) is the volume of CSM, and m (g) is the mass of the sorbent.

2.3.2. Kinetics

The aim of the kinetic experiments is the determination of NH_4^+ sorption kinetic models for CHA μ and CHAg at a temperature of 20 °C. A specific quantity of CHA (0.2 g per $\text{mg NH}_4^+\text{-N L}^{-1}$;

$\cong 123$ g, as indicated by Wasielewski et al. [26]) was added at 0.5 L of CSM and mixed at a constant temperature of 20 °C at a speed of 400 rpm for 420 min. An aliquot of 10 mL was taken at periodic intervals (5, 10, 20, 30, 45, 60, 120, 180, 270, 360, and 420 min) and immediately centrifuged at 4000 rpm for 4 min to separate the solid from the liquid fraction and stop the sorption processes. The batch volume was continuously reduced due to sampling, but it can be assumed that no changes in the ratio of sorbent mass to the volume of CSM occurred because of the homogeneity of the mixture [26]. Experiments were carried out in triplicate and a batch without zeolite (blank) was also included to evaluate air stripping effects. $[\text{NH}_4^+]$ at time t (C_t , mg L^{-1}) and pH were measured in a dilution ratio of 1:20 with Milli-Q water. The time-dependent NH_4^+ adsorption capacity (q_t , mg g^{-1}) was calculated by Equation (1) replacing q_e and C_e with q_t and C_t , respectively. The evaluation of q_e is important in kinetic analyzes to test the validity of the kinetic models applied [37], thus we have considered that a “near-equilibrium” condition was achieved at 420 min from the beginning of the experiment. It is therefore assumed that $q_{t,420} \cong q_e$.

2.4. Equilibrium Isotherms Modelling

The adsorption data were fitted with six different models using the software R Studio [38] with the packages PUPAIM [39] and SorptionAnalysis [40]. Within all the tested equations (Harkins-Jura, Freundlich, Langmuir, Temkin, Fritz-Schlunder, and Dubinin-Radushkevich) we selected the three models that have shown the best correlation with the experimental data, based on R^2 and p-values. The best models were Harkins-Jura, Freundlich, and Langmuir.

2.4.1. Harkins-Jura Isotherm

Harkins-Jura isotherm has been originally proposed for explaining the adsorption of gas molecules, but it has been extended also to liquid–solid systems [41]. It assumes the possibility of multilayer adsorption on the surface of adsorbents having a heterogeneous pore distribution [42]. It has been applied also for a ZRT to describe the adsorption of α , β , and γ -picoline from an aqueous solution [43]. The linear form of the Harkins-Jura model may be expressed by Equation (2) [44]:

$$\frac{1}{q_e^2} = \beta \ln(C_e) + \alpha \quad (2)$$

where q_e is the equilibrium adsorption capacity (mg g^{-1}), C_e is the equilibrium concentration of the sorbate in the liquid phase (mg L^{-1}), and α and β are constants, in particular, α is the intercept and β is the slope which is linked to the specific surface area (S) by Equation (3) [41]:

$$\beta = -\frac{qS^2}{4.606 R T N} \quad (3)$$

where q is a constant dependent on the nature of the adsorbate, R is the universal gas constant, T is temperature and N is the Avogadro number.

2.4.2. Freundlich Isotherm

The Freundlich isotherm is an empirical model that can be used to explain the equilibrium relation between the sorbent and the sorbate for heterogeneous surfaces and in the case of multilayer adsorption [45]. It has been widely used in gas adsorption and environmental soil chemistry [46]. According to Freundlich, the equilibrium adsorption capacity q_e (mg g^{-1}) can be calculated by Equation (4):

$$q_e = K_F \times C_e^{1/n} \quad (4)$$

where K_F is the Freundlich constant ($L g^{-1}$), C_e is the equilibrium concentration ($mg L^{-1}$) and n is constant at a given temperature and it is dependent on the nature of the adsorbate and the adsorbent. A linear form of this expression is given, e.g., by [47] (Equation (5)):

$$\ln(q_e) = n^{-1} \ln(C_e) + \ln(K_F) \quad (5)$$

2.4.3. Langmuir Isotherm

The Langmuir model [48] assumes that only one layer of the adsorbate is formed (monolayer assumption) and that the energetic properties of the adsorption sites are equivalent. Due to the formation of a monolayer, the Langmuir model provides a “flat” region which permits the determination of the maximum adsorption capacity q_{max} ($mg g^{-1}$) (Equation (6)):

$$q_e = \frac{q_{max} K_L C_e}{1 + K_L C_e} \quad (6)$$

where q_e is the equilibrium adsorption capacity ($mg g^{-1}$), K_L is the Langmuir constant ($L mg^{-1}$) and C_e is the concentration at equilibrium ($mg L^{-1}$). A linear form of this expression is given, e.g., by Equation (7) [26]:

$$\frac{1}{q_e} = \frac{1}{q_{max} K_L} \frac{1}{C_e} + \frac{1}{q_{max}} \quad (7)$$

2.5. Kinetic Models

Adsorption involves multiple processes as (i) diffusion across the liquid phase near the solid surfaces, (ii) diffusion through the pore structure of the sorbent (Intraparticle Diffusion, ID), and physical and chemical bonding on the solid surfaces [49].

Kinetic data were analyzed using the Pseudo-First-Order, Pseudo-Second-Order, Intraparticle Diffusion, and Elovich equations. As pointed out by [37], for kinetic investigations it is appropriate to take into account only data sufficiently far from equilibrium, and for this reason only data with a fractional uptake $F(t) < 85\%$ were considered. $F(t)$ was calculated by Equation (8) [37]:

$$F(t) = q(t)/q_e \quad (8)$$

2.5.1. Pseudo-First-Order

The Pseudo-First-Order model (PFO), proposed by [50] can be described in its linear form by Equation (9) [51]:

$$\ln(q_e - q_t) = \ln(q_e) - k_1 t \quad (9)$$

where q_e and q_t are the equilibrium adsorption capacity and the adsorption capacity at time t ($mg g^{-1}$); in particular $(q_e - q_t)$ has been called “driving force” [52] and is proportional to the available fraction of active sites. t is the contact time (min) and k_1 is the PFO rate constant (min^{-1}). If kinetic data are explainable with the PFO model, the plot of $\ln(q_e - q_t)$ against t describes a straight line with a slope equal to $-k_1/2.303$ and an intercept equal to $\ln(q_e)$ [53].

2.5.2. Pseudo-Second-Order

The Pseudo-Second-Order equation (PSO) can be expressed in linear form by Equation (10) [54]:

$$\frac{t}{q_t} = \frac{1}{q_e} t + \frac{1}{h} \quad (10)$$

where t is time (min), q_t is the time-dependent adsorption capacity ($mg g^{-1}$), q_e is the equilibrium sorption capacity ($mg g^{-1}$) and h is the initial adsorption rate ($mg g^{-1} min^{-1}$).

The PSO rate constant k_2 is obtainable by Equation (11) [54]:

$$k_2 = \frac{h}{q_e^2} \quad (11)$$

All the parameters are experimentally determinable from the slope and the intercept of plot t/q_t against t [55–57].

2.5.3. Intra-Particle Diffusion

The intra-particle diffusion (ID) equation describes a diffusion-controlled process [58,59] using Equation (12) [26]:

$$q_t = k_{ID}t^{0.5} + C \quad (12)$$

where K_{ID} is the intra-particle diffusion rate constant.

Plotting q_t against $t^{0.5}$ gives a linear correlation where the intercept C is proportional to the thickness of the boundary layer [57], and the slope is equal to K_{ID} . If $C \cong 0$, it can be assumed that sole intra-particle diffusion occurs [26]. If the experimental data shows the presence of two or more separate regions, a multistage diffusion process is present where the first step represents the external surface adsorption and/or macropore diffusion [57].

2.5.4. Elovich Kinetic Model

The Elovich equation was historically applied to determine the kinetics in the chemisorption of gases onto heterogeneous solids [52,60]; starting twenty years ago, the Elovich model has been applied to describe the adsorption process of different pollutants from aqueous solutions [61,62]; in 2004, Cortés and Martínez [63] applied this model on natural zeolites, to describe the sorption kinetics of cadmium (II) from solution. The model can be described by Equation (13) [53]:

$$\frac{dq_t}{dt} = a \exp(-\alpha q_t) \quad (13)$$

where q_t is the time-dependent sorption capacity, a and α are constants, and, in particular, α corresponds to the initial adsorption rate. A linear form is given by Equation (14) [54]:

$$q_t = \left(\frac{2.3}{\alpha}\right) \ln(t + t_0) - \left(\frac{2.3}{\alpha}\right) \ln(t_0) \quad (14)$$

Using the dimensionless Elovich model (Equation (15)) it is possible to calculate R_E which is an approaching-equilibrium parameter representing the velocity of the system to arrive at equilibrium conditions [64]:

$$\frac{q_t}{q_{ref}} = R_E \ln\left(\frac{t}{t_{ref}}\right) + 1 \quad (15)$$

where t_{ref} is the longest operating time in the adsorption process (min) and q_{ref} is the amount of adsorption at time $t = t_{ref}$ (mg g^{-1}).

2.6. Thermodynamic Calculations

Thermodynamic parameters were calculated for CHA μ and CHAg at the temperatures of 286, 293, and 310 K (13, 20 and 37 °C), respectively.

The thermodynamic equilibrium constant (K_e) is the ratio of q_e against C_e when C_e tends to zero (Equation (16)) and it is possible to obtain by plotting q_e/C_e against C_e and extrapolating the value of the intercept at $C_e = 0$ [65]:

$$\lim_{C_e \rightarrow 0} \frac{q_e}{C_e} = K_e \quad (16)$$

Analyzing the variation of K_e with temperature, it is possible to obtain the change in standard enthalpy (ΔH , J mol⁻¹) and the change in standard entropy (ΔS , J K⁻¹ mol⁻¹) through the application of the van 't Hoff isochore (Equation (17)) [27]:

$$\ln(K_e) = -\frac{\Delta H}{R} \frac{1}{T} + \frac{\Delta S}{R} \quad (17)$$

where R is the universal gas constant (J K⁻¹ mol⁻¹) and T is the temperature (K). ΔH and ΔS may be obtained by the linear regression of $\ln(K_e)$ against $1/T$, whose slope is equal to $-\Delta H/R$ and its intercept is equal to $\Delta S/R$ [26]. It is important to note that ΔH and ΔS are independent of temperature.

The Gibbs free surface energy change (ΔG , J mol⁻¹), was then determined by the application of two approaches: Equation (18) and the Gibbs-Helmholtz equation (Equation (19)). The values obtained by the two methods were slightly different and these differences were due to the previous linear regression steps.

$$\Delta G = -RT \ln(K_e) \quad (18)$$

$$\Delta G = \Delta H - T\Delta S \quad (19)$$

3. Results and Discussions

3.1. Isotherms

The plots of q_e against C_e are reported in Figure 1. All the parameters of Harkins-Jura, Freundlich, and Langmuir isotherms are reported in Table 1.

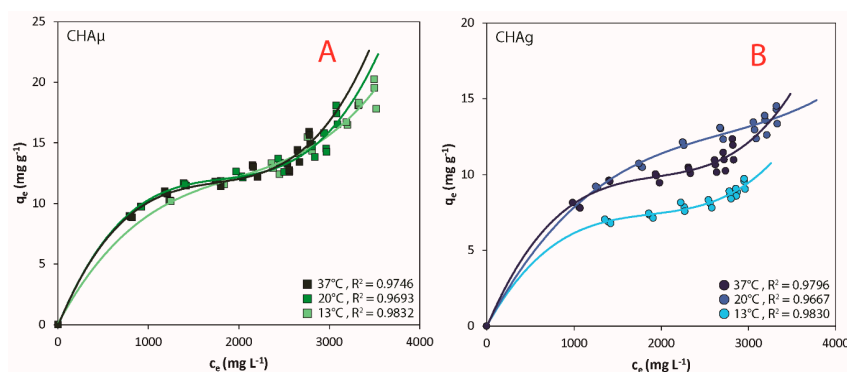


Figure 1. Equilibrium adsorption capacity q_e (mg g⁻¹) against equilibrium concentration C_e (mg L⁻¹) after a contact time of 20 h with centrifuged swine manure (CSM): (A) trends for CHA μ (3rd degree polynomials) at 13, 20, and 37 °C and respective R² values; (B) trends for CHAg (3rd degree polynomials) at 13, 20 and 37 °C and respective R² values. Both CHA μ and CHAg have shown an equilibrium trend of the L3 type following the classification proposed by Giles et al. [66].

Table 1. Parameters calculated by Harkins-Jura, Freundlich, and Langmuir isotherms (Equation (2), Equation (4) and Equation (7) respectively) for CHA μ and CHAg, at temperatures T = 286, 293, and 307 K (13, 20 and 37 °C). Initial pH and NH₄⁺ load were 8.07 ± 0.03 and 3140 ± 45 mg L⁻¹ respectively.

Sorbent	Temperature		Harkins-Jura		Freundlich			Langmuir		
	T	R ²	α	β	R ²	K_F	n	R ²	K_L	q_{max}
	(K)	(-)	(g ² mg ⁻²)	(g ² L mg ⁻³)	(-)	(L g ⁻¹)	(-)	(-)	(L mg ⁻¹)	(mg g ⁻¹)
CHA μ	286	0.973	0.057	-0.015	0.904	0.14	1.67	0.878	3.98×10^{-4}	29.5
	293	0.931	0.045	-0.012	0.853	0.66	2.55	0.860	10.27×10^{-4}	19.6
	310	0.920	0.051	-0.013	0.896	0.77	2.71	0.911	12.03×10^{-4}	18.1
CHAg	286	0.876	0.109	-0.028	0.826	0.45	2.68	0.798	9.12×10^{-4}	12.0
	293	0.937	0.057	-0.015	0.937	0.56	2.55	0.954	7.40×10^{-4}	18.9
	310	0.826	0.063	-0.016	0.826	0.95	3.23	0.843	13.03×10^{-4}	14.0

The shape of the curves in the first region of the graphs indicates that, as more exchange sites are occupied by NH_4^+ , it becomes increasingly difficult for other NH_4^+ in solution to find and substitute exchangeable counterions. The presence of a semi-flat region, located in the middle of the graphs, means that a saturation condition is beginning to occur associated with the formation of an adsorption monolayer but, since the end of the curve rises again, it demonstrates a renewed availability of exchange sites for NH_4^+ adsorption [66]. This behavior was observed for both CHA_μ and CHAg and it starts approximately when 3 g of ZRT was added to 50 mL of CSM (6 wt%).

The formation of more than one adsorption layer is not in agreement with the Langmuir monolayer assumption [44] because the Langmuir model assumes the existence of a horizontal asymptote that determines the maximum adsorption capacity, q_{max} . R^2 values have in general shown worse correlations for Langmuir compared to the other isotherm models.

The Freundlich model is commonly utilized to explain adsorption for heterogeneous materials. n is a heterogeneity parameter that, if higher than 0, indicates surface heterogeneity [67]. For all the isotherms investigated in CHA_μ and CHAg , n is greater than 0 demonstrating the heterogeneous nature of the adsorption surfaces. It is likely to expect a certain degree of inhomogeneity in the adsorbent because the used ZRT is a natural material with significant differences both in particle size and in its mineralogy (see Section 2.1). Freundlich isotherms assume an asymptotic maximum, without reaching a maximum adsorption capacity (q_{max}), as for the Langmuir model, but the isotherms in Figure 1 do not tend to linearize in the right portion of the graph, suggesting that the Freundlich equation cannot explain in this case the experimental observations.

The applicability of Harkins-Jura is demonstrated by obtaining straight lines in the plot $\ln(C_e)$ against $1/q_e^2$. Within the model tested, the best R^2 values were in general obtained with the Harkins-Jura isotherm (Figure 2, Table 1). Within the Harkins-Jura model, two distinct straight lines can be obtained, whose intersection point corresponds to the completion of the adsorption monolayer [41]. Here, two distinct lines have not been clearly observed, but the points of some isotherms, as CHAg 13 °C and CHAg 37 °C, tend to flex downward in the rightmost part of the graph (Figure 2B). Their flexion corresponds to an equilibrium concentration $C_e \approx 2700 \text{ mg L}^{-1}$, which represents a condition where the monolayer is “almost complete” and, beyond which, an adsorption multilayer is developed allowing a rapid increase in the adsorption capacity q_e (Figure 1B).

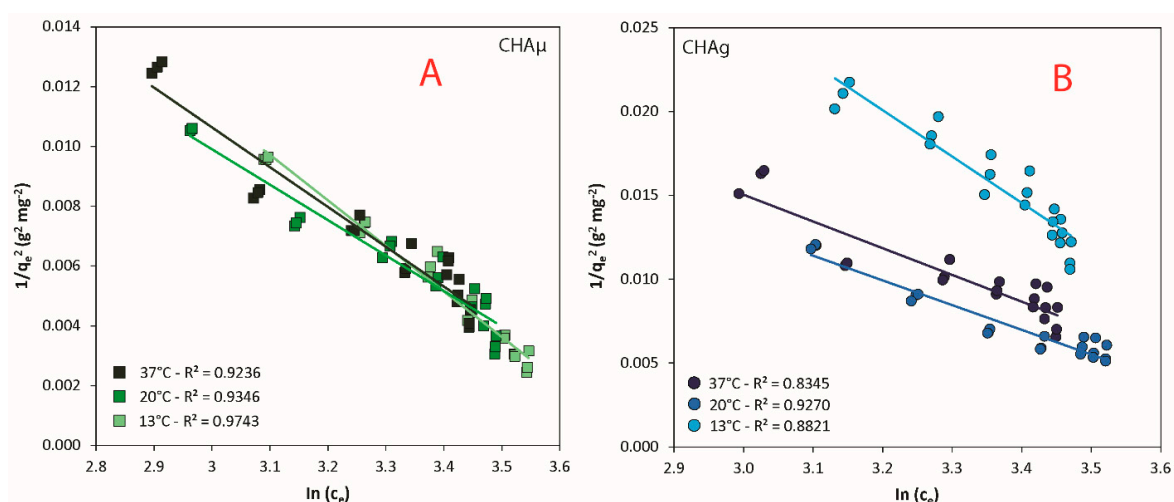


Figure 2. $\ln(C_e)$ against $1/q_e^2$ (Linear Harkins-Jura isotherms; Equation (2)) for CHA_μ and CHAg at temperatures $T = 13, 20,$ and 37 °C: (A) Isotherms for CHA_μ at the temperature investigated and with the respective R^2 values; (B) Isotherms for CHAg at the temperature investigated and with the respective R^2 values.

Regarding the effects of temperature on the NH_4^+ adsorption at equilibrium, the isotherms of CHA_μ are very close to each other, indicating that there is not a significant temperature effect for

CHA μ (Figure 2A). On the other hand, CHAg sorption was much more dependent on temperature (Figure 2B) and the best adsorption performances occurred at 20 °C whereas the worst occurred at 13 °C. Therefore, from the experimental data, it seems that temperature has increasing effects on NH $_4^+$ adsorption as the particle size increases. An explanation of this phenomenon is particularly difficult to provide with the collected data, taking also into account that, to the best of the author’s knowledge, there are no scientific publications yet on how temperature affects adsorption on different particle sizes. Alshameri et al. [68] has observed ambiguous effects of temperature on NH $_4^+$ adsorption by a natural clinoptilolite. The NH $_4^+$ removal increased from 25 to 35 °C, but it decreased from 35 to 45 °C. Here also the effect of temperature on CHAg is ambiguous, but it is clear that the worst adsorption capacities were reached at the lower temperature (13 °C).

3.2. Kinetics

Kinetic parameters calculated from PFO, PSO, and Elovich equations are reported in Table 2 while q_t versus t , PSO, and Elovich graphs are reported in Figure 3.

Table 2. Pseudo-First-Order model (PFO), Pseudo-Second-Order Equation (PSO), and Elovich parameters for CHA μ and CHAg and the relative R 2 values.

Sorbent	PFO			PSO			Elovich			
	R 2 (-)	k_1 (min $^{-1}$)	$q_{e,1}$ (mg g $^{-1}$)	R 2 (-)	k_2 (g mg $^{-1}$ min $^{-1}$)	$q_{e,2}$ (mg g $^{-1}$)	h (mg g $^{-1}$ min $^{-1}$)	R 2 (-)	α (mg g $^{-1}$ min $^{-1}$)	R $_E$ (-)
CHA μ	0.779	0.0104	5.39	0.988	0.065	6.41	2.667	0.921	1.01	0.282
CHAg	0.814	0.0036	6.67	0.977	0.018	5.61	0.566	0.985	0.82	0.407

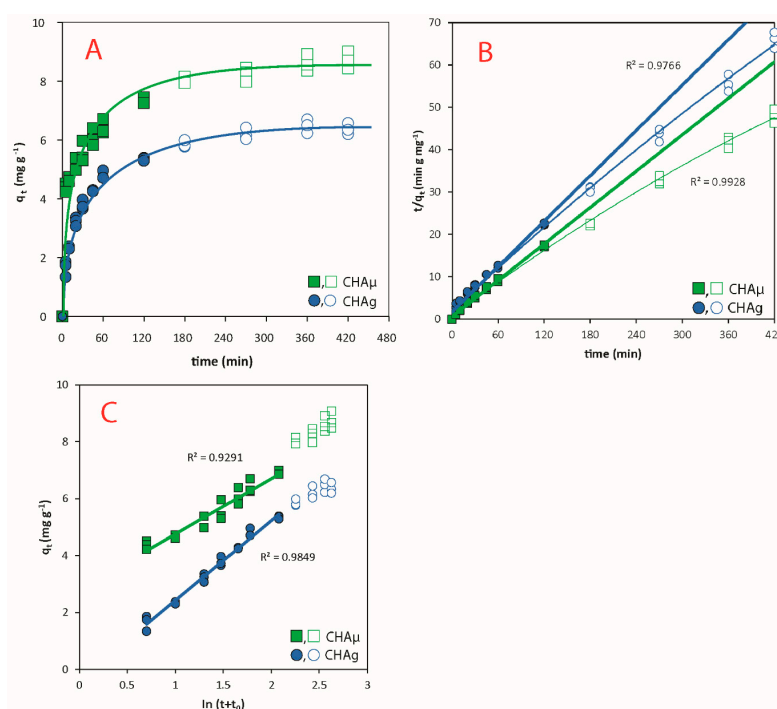


Figure 3. Kinetic graphics; full dots are data with $F(t) < 85\%$, thus they have been considered in kinetic analyzes; empty dots are data with $F(t) > 85\%$, thus they were not taken into consideration: (A) q_t against t plot for CHA μ and CHAg; the curve indicates the general trend with respect to time; (B) PSO plot (t/q_t against t) thinner lines are representing the trend of all data; straight regression lines are the PSO linear equations (Equation (10)); (C) Elovich plot ($\ln(t+t_0)$ versus q_t); straight lines represent the Elovich linear equation (Equation (14)).

To verify the goodness of PFO and PSO models, in addition to the evaluation of R^2 , it is necessary also to make a comparison between the q_e calculated by the models and the q_e experimentally measured.

In kinetic experiments, a “close-to-equilibrium” condition was assumed at $t = 420$ min (see Section 2.3.2) and the q_e measured were 8.74 and 6.37 mg g^{-1} for CHA μ and CHAg respectively.

The PSO model showed high R^2 values, but q_e calculated ($q_{e,2}$) are quite different from the measured values, thus kinetics can not be explained using the PSO equation. The Elovich model has shown a good correlation with the experimental data, in particular regarding CHAg. R_E values indicate that the velocities of the systems to reach an equilibrium condition are different between the two different particle sizes. In particular, CHAg approaches equilibrium conditions more slowly than CHA μ [64]. A plausible explanation for the differences observed in adsorption velocities between the two particle sizes may relate to the structural differences derived from the grinding process that, undoubtedly, increased the specific surface area of CHA μ compared to CHAg and compromised, at least in part, the intercrystalline macroporous structure of the tuff. The grinding process which CHA μ has undergone did not destroy the porous structure of the zeolite because, even if it is a micro-sized material, the size of CHA μ was about 10^3 times larger than the average diameter of the micropores of chabazite [69]. It is instead plausible that the crushing process has exposed to the environment a larger number of openings into which NH_4^+ can easily enter, increasing the ion-exchange probability for a given NH_4^+ ion in solution and explaining CHA μ 's higher adsorption rates than CHAg.

Diffusion dynamics of NH_4^+ has shown different behaviours when comparing CHAg and CHA μ (Figure 4); in particular, the ID plot for CHA μ has shown only a straight line with an intercept $C \sim 4$, while CHAg has shown two lines, correlated with a rapid change of NH_4^+ diffusion which begins after about 60 min of contact with CSM.

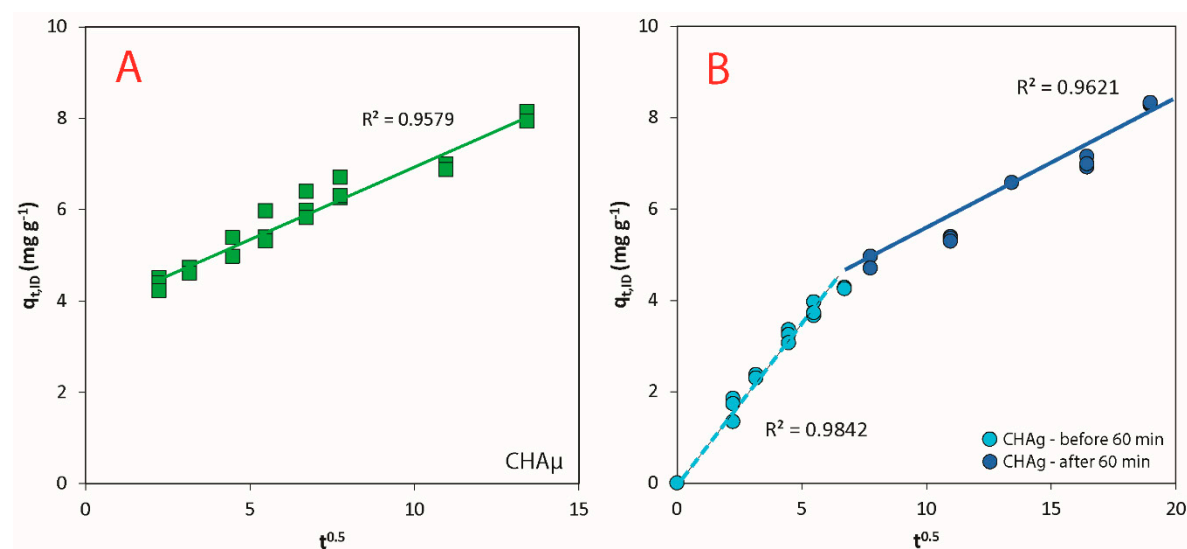


Figure 4. ID plots ($t^{0.5}$ against $q_{t, ID}$, Equation (12)): (A) linear regression for CHA μ with relative R^2 ; (B) ID model for CHAg; the leftmost line represent data before the first hour of contact while in the rightmost part there are data after the first 60 min; the graph shows two distinct regions with different ID parameters; R^2 values are reported.

In the first region of the CHAg plot (Figure 4B), which represents about the first 60 min of contact with CSM, the intercept value is near zero ($C = 0.17$), demonstrating that the adsorption was mainly governed by ID process. During the first hour, external-surface adsorption and macropore diffusion occurred and a thin boundary layer has developed, as indicated by the low value of $C = 0.17$ which is proportional to the thickness of the boundary layer [57]. After one hour, adsorption layers thickened significantly ($C = 2.24$) and NH_4^+ penetrated more slowly inside the internal structure and the micropores.

ID plot for CHA μ (Figure 4A) shows only a line with a not very steep slope ($K_{ID} = 0.32$) and similar to the slope of CHAg after the first hour of contact ($K_{ID} = 0.31$). The high C value ($C = 3.75$) indicates the formation of a thick adsorption layer. It is likely that, in this case, the first diffusion in the external surface and through the macropore structure was really fast; the experimental data has not allowed the observation of a steep line corresponding to the first minutes of contact, but it was plausibly present before the first five minutes of contact with CSM.

ID parameters are reported in Table 3.

Table 3. ID parameters for CHA μ and CHAg; CHAg has two distinct patterns, before and after 60 min of contact with CSM.

Sorbent		ID Model		
		R^2	K_{ID}	C
		(-)	($\text{mg g}^{-1} \text{min}^{-0.5}$)	(mg g^{-1})
CHA μ		0.958	0.32	3.75
CHAg	Before 60 min.	0.984	0.63	0.17
	After 60 min.	0.962	0.31	2.24

3.3. Thermodynamics

The thermodynamic parameters of K_e , ΔG_1 , and ΔG_2 are reported in Table 4. The ΔG values obtained by Equation (18) and Equation (19) are similar, demonstrating little discrepancies between the two approaches adopted. ΔG is always negative, indicating that NH_4^+ adsorption was a spontaneous process for all the sizes tested and for all the working temperatures. NH_4^+ adsorption by CHA μ is thermodynamically favored rather than CHAg, as indicated by its general lowest values of ΔG . Temperature has a positive effect on ΔG which at higher temperatures reaches the lowest values.

Table 4. Thermodynamic parameters of K_e (Equation (16)) and ΔG calculated by Equation (18) (ΔG_1) and Equation (19) (ΔG_2) for CHA μ and CHAg, at the temperatures of 286, 293, and 310 K (13, 20 and 37 °C, respectively); see paragraph 2.6 for details.

Thermodynamic Parameters		CHA μ			CHAg		
		Temperature (°C)					
		13	20	37	13	20	37
K_e	(-)	8.83	11.80	12.61	6.25	8.86	9.60
ΔG_1	(J mol^{-1})	-2251	-2613	-2839	-1893	-2310	-2533
ΔG_2	(J mol^{-1})	-2333	-2492	-2878	-1992	-2164	-2581

K_e has positive values for all CHA μ and CHAg, indicating that the equilibrium between NH_4^+ adsorption and desorption (represented by q_e and C_e respectively in Equation (16)) is shifted towards the adsorption process. The grain size of the adsorbent affected K_e , indeed CHA μ has shown greater values than CHAg, meaning that the micro-sized ZRT has favored the adsorption more than the granular one. This consideration is also supported by q_e against C_e graphs (see Figure 1, Section 3.1), where it can be seen that the best performances have been achieved by CHA μ instead of CHAg.

The values of ΔH and ΔS are reported in Table 5. ΔS were positive, indicating that the randomness in the solid-liquid interface increased, reflecting a good affinity between the sorbent and the sorbate and a condition that favors the occurrence of the adsorption processes [70]. ΔH is positive for both CHA μ and CHAg indicating that NH_4^+ adsorption was an endothermic process, with significative higher values for CHAg. Endothermy is also supported by the Freundlich constant K_F that increased with increasing temperature (see Table 1, Section 3.1) [71].

Table 5. Thermodynamic parameters of ΔH and ΔS for CHA μ and CHAg; see Section 2.6 for details.

Thermodynamic Parameters	CHA μ	CHAg
ΔH (J mol ⁻¹)	4174	5036
ΔS (J K ⁻¹ mol ⁻¹)	22.7	24.6

While many authors have observed exothermic conditions for NH₄⁺ adsorption onto ZRT ($\Delta H < 0$) [27,29,72], others have calculated positive values of ΔH [26,57]. In all these studies, the nature of the employed materials (the type of ZRT and type of the liquid phase) varies significantly and this may result in differences in the adsorption processes, thus explaining this variability in the thermodynamic parameters.

4. Conclusions

In this work, the adsorption of ammonium ions from a raw liquid swine manure by a chabazite zeolite-rich tuff was characterized. The equilibrium curve was of L3 type following the isotherms classification by Giles et al. [66], suggesting that a multilayer adsorption condition has occurred. Due to the multilayer formation, the maximum adsorption capacities were obtained using low dosages of adsorbent (<6 wt%). A clear temperature effect was not observed for the micronized zeolite tuff while the coarser particle size showed poorer performance at lower temperatures. Particle size was an important aspect that influenced both the velocity of adsorption, the equilibrium conditions, and the thermodynamic. Intraparticle diffusion had a major control on the overall adsorption rate. Zeolites are microporous selective ion exchangers, thus diffusion of the counterions (both the adsorbed and the desorbed ones) is an essential process that controls and limits the ion exchange. Generally, the highest adsorption capacities and adsorption rates were achieved using the micronized zeolite-rich tuff.

The outcomes of this work highlighted the complexity of sorption mechanisms in raw liquid animal manure and proved that the use of chabazite zeolite-rich tuff is a valid technology for the recycling of N.

Author Contributions: Conceptualization, G.G. and G.F.; methodology, G.G. and G.F.; formal analysis, G.G., G.F., V.M., N.T.; investigation, G.G.; resources, B.F. and M.C.; data curation, G.G.; writing—original draft preparation, G.G.; writing—review and editing, G.F., B.F., M.C.; supervision, G.F., M.C. All authors have read and agreed to the published version of the manuscript.

Funding: We kindly thank the Emilia Romagna Region for the PhD grant inherent to the research project “Innovative geomaterials for the reduction of nitrogen load in livestock and industrial wastewater”, specified by Deliberation n°. 769 of 21/05/2018, B area) “Human resources for intelligent specialization”.

Acknowledgments: We gratefully thank Miotto Giuliano for supplying the liquid animal manure and Verdi S.p.a. for the furnishing of the zeolite-rich tuff.

Conflicts of Interest: The authors declare no conflict of interest.

References

1. FAO. How to Feed the World in 2050. In Proceedings of the Expert Meeting on How to Feed the World in 2050, Rome, Italy, 24–26 June 2009.
2. Dawson, J.C.; Huggins, D.R.; Jones, S.S. Characterizing nitrogen use efficiency in natural and agricultural ecosystems to improve the performance of cereal crops in low-input and organic agricultural systems. *Field Crop. Res.* **2008**, *107*, 89–101. [[CrossRef](#)]
3. Afreh, D.; Zhang, J.; Guan, D.; Liu, K.; Song, Z.; Zheng, C.; Deng, A.; Feng, X.; Zhang, X.; Wu, Y.; et al. Long-term fertilization on nitrogen use efficiency and greenhouse gas emissions in a double maize cropping system in subtropical China. *Soil Tillage Res.* **2018**, *180*, 259–267. [[CrossRef](#)]
4. Smith, K.A.; Jackson, D.R.; Pepper, T.J. Nutrient losses by surface run-off following the application of organic manures to arable land. 1. Nitrogen. *Environ. Pollut.* **2001**, *112*, 41–51. [[CrossRef](#)]
5. Andersen, H.E.; Kronvang, B.; Larsen, S.E. Agricultural practices and diffuse nitrogen pollution in Denmark: Empirical leaching and catchment models. *Water Sci. Technol.* **1999**, *39*, 257–264. [[CrossRef](#)]

6. Carpenter, S.R.; Caraco, N.F.; Correll, D.L.; Howarth, R.W.; Sharples, A.N.; Smith, V.H. Nonpoint pollution of surface waters with phosphorus and nitrogen. *Ecol. Appl.* **1998**, *8*, 559–568. [[CrossRef](#)]
7. Choudhury, A.T.M.A.; Kennedy, I.R. Nitrogen fertilizer losses from rice soils and control of environmental pollution problems. *Commun. Soil Sci. Plant Anal.* **2005**, *36*, 1625–1639. [[CrossRef](#)]
8. Bijay-Singh; Yadvinder-Singh; Sekhon, G.S. Fertilizer-N use efficiency and nitrate pollution of groundwater in developing countries. *J. Contam. Hydrol.* **1995**, *20*, 167–184. [[CrossRef](#)]
9. Majumdar, D. Nitrate pollution of groundwater and associated human health disorders. *Indian J. Environ. Health* **2000**, *42*, 28–39.
10. Faccini, B.; Di Giuseppe, D.; Malferrari, D.; Coltorti, M.; Abbondanzi, F.; Campisi, T.; Laurora, A.; Passaglia, E. Ammonium-exchanged zeolite preparation for agricultural uses: From laboratory tests to large-scale application in ZeoLIFE project prototype. *Period. Mineral.* **2015**, *84*, 303–321. [[CrossRef](#)]
11. Ferretti, G.; Di Giuseppe, D.; Natali, C.; Faccini, B.; Bianchini, G.; Coltorti, M. C-N elemental and isotopic investigation in agricultural soils: Insights on the effects of zeolite amendments. *Chem. Erde.* **2017**, *77*, 45–52. [[CrossRef](#)]
12. Faccini, B.; Di Giuseppe, D.; Ferretti, G.; Coltorti, M.; Colombani, N.; Mastrocicco, M. Natural and NH_4^+ -enriched zeolite amendment effects on nitrate leaching from a reclaimed agricultural soil (Ferrara Province, Italy). *Nutr. Cycl. Agroecosyst.* **2018**, *110*, 327–341. [[CrossRef](#)]
13. Galli, E.; Passaglia, E. Natural zeolites in environmental engineering. In *Zeolites in Chemical Engineering*; Holzapfel, H., Ed.; Verlag ProcessEng Engineering GmbH: Vienna, Austria, 2011; pp. 392–416. ISBN 3902655089.
14. Baerlocher, C.; McCusker, L.B. (Eds.) Chapter 3 Zeolite structures. In *Studies in Surface Science and Catalysis 137*; Elsevier: Amsterdam, The Netherlands, 2001; pp. 37–67.
15. Cejka, J.; Van Bekkum, H.; Corma, A.; Schüth, F. *Studies in Surface Science and Catalysis 168: Introduction to Zeolite Science and Practice*; Elsevier: Amsterdam, The Netherlands, 2007; Volume 168, ISBN 978-0-444-53063-9.
16. Dyer, A.; Zubair, M. Ion-exchange in chabazite. *Microporous Mesoporous Mater.* **1998**, *22*, 135–150. [[CrossRef](#)]
17. Eslami, M.; Khorassani, R.; Coltorti, M.; Malferrari, D.; Faccini, B.; Ferretti, G.; Di Giuseppe, D.; Fotovat, A.; Halajnia, A. Leaching behaviour of a sandy soil amended with natural and NH_4^+ and K^+ saturated clinoptilolite and chabazite. *Arch. Agron. Soil Sci.* **2018**, *64*, 1142–1151. [[CrossRef](#)]
18. Ferretti, G.; Keiblinger, K.M.; Di Giuseppe, D.; Faccini, B.; Colombani, N.; Zechmeister-Boltenstern, S.; Coltorti, M.; Mastrocicco, M. Short-Term Response of Soil Microbial Biomass to Different Chabazite Zeolite Amendments. *Pedosphere.* **2018**, *28*, 277–287. [[CrossRef](#)]
19. Di Giuseppe, D.; Ferretti, G.; Faccini, B.; Blasi, E.; Passeri, N.; Bianchini, G.; Coltorti, M. Is it possible to cultivate corn in a sustainable way using a quarry waste? *Period. Mineral.* **2016**, *85*, 179–183. [[CrossRef](#)]
20. Ferretti, G.; Keiblinger, K.M.; Zimmermann, M.; Di Giuseppe, D.; Faccini, B.; Colombani, N.; Mentler, A.; Zechmeister-Boltenstern, S.; Coltorti, M.; Mastrocicco, M. High resolution short-term investigation of soil CO_2 , N_2O , NO_x and NH_3 emissions after different chabazite zeolite amendments. *Appl. Soil Ecol.* **2017**, *119*, 138–144. [[CrossRef](#)]
21. Ferretti, G.; Faccini, B.; Vittori Antisari, L.; Di Giuseppe, D.; Coltorti, M. ^{15}N Natural Abundance, Nitrogen and Carbon Pools in Soil-Sorghum System Amended with Natural and NH_4^+ -Enriched Zeolites. *Appl. Sci.* **2019**, *9*, 4524. [[CrossRef](#)]
22. Polat, E.; Karaca, M.; Demir, H.; Onus, A.N. Use of Natural Zeolite (Clinoptilolite) in Agriculture. *J. Fruit Ornam. Plant Res.* **2004**, *12*, 183–189.
23. Mastinu, A.; Kumar, A.; Maccarinelli, G.; Bonini, S.A.; Premoli, M.; Aria, F.; Gianoncelli, A.; Memo, M. Zeolite clinoptilolite: Therapeutic virtues of an ancient mineral. *Molecules* **2019**, *24*, 1517. [[CrossRef](#)]
24. Moshoeshe, M.; Silas Nadiye-Tabbiruka, M.; Obuseng, V. A Review of the Chemistry, Structure, Properties and Applications of Zeolites. *Am. J. Mater. Sci.* **2017**, *2017*, 196–221. [[CrossRef](#)]
25. Huang, H.; Xiao, X.; Yan, B.; Yang, L. Ammonium removal from aqueous solutions by using natural Chinese (Chende) zeolite as adsorbent. *J. Hazard. Mater.* **2010**, *175*, 247–252. [[CrossRef](#)] [[PubMed](#)]
26. Wasielewski, S.; Rott, E.; Minke, R.; Steinmetz, H. Evaluation of Different Clinoptilolite Zeolites as Adsorbent for Ammonium Removal from Highly Concentrated Synthetic Wastewater. *Water* **2018**, *10*, 584. [[CrossRef](#)]

27. Gunay, A. Application of nonlinear regression analysis for ammonium exchange by natural (Bigadiç) clinoptilolite. *J. Hazard. Mater.* **2007**, *148*, 708–713. [[CrossRef](#)] [[PubMed](#)]
28. Jha, V.K.; Hayashi, S. Modification on natural clinoptilolite zeolite for its NH_4^+ retention capacity. *J. Hazard. Mater.* **2009**, *169*, 29–35. [[CrossRef](#)] [[PubMed](#)]
29. Saltali, K.; Sari, A.; Aydin, M. Removal of ammonium ion from aqueous solution by natural Turkish (Yıldızeli) zeolite for environmental quality. *J. Hazard. Mater.* **2007**, *141*, 258–263. [[CrossRef](#)]
30. Chen, H.-F.; Lin, Y.-J.; Chen, B.-H.; Yoshiyuki, I.; Liou, S.; Huang, R.-T. A Further Investigation of NH_4^+ Removal Mechanisms by Using Natural and Synthetic Zeolites in Different Concentrations and Temperatures. *Minerals*. **2018**, *8*, 499. [[CrossRef](#)]
31. Nguyen, M.L.; Tanner, C.C. Ammonium removal from wastewaters using natural New Zealand zeolites. *N. Z. J. Agric. Res.* **2010**, *41*, 427–446. [[CrossRef](#)]
32. Moussavi, G.; Talebi, S.; Farrokhi, M.; Sabouti, R.M. The investigation of mechanism, kinetic and isotherm of ammonia and humic acid co-adsorption onto natural zeolite. *Chem. Eng. J.* **2011**, *171*, 1159–1169. [[CrossRef](#)]
33. Cheng, Q.; Li, H.; Xu, Y.; Chen, S.; Liao, Y.; Deng, F.; Li, J. Study on the adsorption of nitrogen and phosphorus from biogas slurry by NaCl-modified zeolite. *PLoS ONE* **2017**, *12*, e0176109. [[CrossRef](#)]
34. Malferrari, D.; Laurora, A.; Brigatti, M.F.; Coltorti, M.; Di Giuseppe, D.; Faccini, B.; Passaglia, E.; Vezzalini, M.G. Open-field experimentation of an innovative and integrated zeolitite cycle: Project definition and material characterization. *Rend. Lincei*. **2013**, *24*, 141–150. [[CrossRef](#)]
35. Li, M.; Zhu, X.; Zhu, F.; Ren, G.; Cao, G.; Song, L. Application of modified zeolite for ammonium removal from drinking water. *Desalination*. **2011**, *271*, 295–300. [[CrossRef](#)]
36. Guo, X.; Zeng, L.; Li, X.; Park, H.S. Ammonium and potassium removal for anaerobically digested wastewater using natural clinoptilolite followed by membrane pretreatment. *J. Hazard. Mater.* **2008**, *151*, 125–133. [[CrossRef](#)]
37. Simonin, J.P. On the comparison of pseudo-first order and pseudo-second order rate laws in the modeling of adsorption kinetics. *Chem. Eng. J.* **2016**, *300*, 254–263. [[CrossRef](#)]
38. R Core Team. RStudio. 2019. Available online: <https://rstudio.com/products/rstudio/download/> (accessed on 9 December 2019).
39. Saroyda, J.R.V.; Cruz, R.Y.S.; Antonio, R.J.C.; Flestado, C.L.P.; Magalong, J.R.S.; Zagala, K.Z.P.; Barbacena, C.L.; Bumatay, J.M.; Bautista, L.F.; Deocarís, C.C. PUPAIM. 2001. Available online: <https://cran.r-project.org/package=PUPAIM> (accessed on 10 May 2019).
40. Chattopadhyay, A. Sorption Analysis: Static Adsorption Experiment Plotting and Analysis. 2017. Available online: <https://cran.r-project.org/package=SorptionAnalysis> (accessed on 10 May 2019).
41. Iyer, K.P.D.; Kunju, A.S. Extension of Harkins-Jura adsorption isotherm to solute adsorption. *Colloids Surf.* **1992**, *63*, 235–240. [[CrossRef](#)]
42. Harkins, W.D.; Jura, G. The decrease (π) of free surface energy (γ) as a basis for the development of equations for adsorption isotherms; And the existence of two condensed phases in films on solids. *J. Chem. Phys.* **1944**, *12*, 112–113. [[CrossRef](#)]
43. Rawajfih, Z.; Al Mohammad, H.; Nsour, N.; Ibrahim, K. Study of equilibrium and thermodynamic adsorption of α -picoline, β -picoline, and γ -picoline by Jordanian zeolites: Phillipsite and faujasite. *Microporous Mesoporous Mater.* **2010**, *132*, 401–408. [[CrossRef](#)]
44. Shanavas, S.; Salahuddin Kunju, A.; Varghese, H.T.; Yohannan Panicker, C. Comparison of Langmuir and Harkins-Jura Adsorption Isotherms for the Determination of Surface Area of Solids: Oriental Journal of Chemistry. *Orient. J. Chem.* **2011**, *27*, 245–252.
45. Ho, Y.S.; McKay, G. Application of Kinetic Models to the Sorption of Copper(II) on to Peat. *Adsorpt. Sci. Technol.* **2002**, *20*, 797–815. [[CrossRef](#)]
46. Sparks, D.L. *Environmental Soil Chemistry*, 2nd ed.; Academic Press: Cambridge, MA, USA, 2002; ISBN 9780080494807.
47. Subramanyam, B.; Das, A. Linearised and non-linearised isotherm models optimization analysis by error functions and statistical means. *J. Environ. Heal. Sci. Eng.* **2014**, *12*. [[CrossRef](#)] [[PubMed](#)]

48. Langmuir, I. The adsorption of gases on plane surfaces of glass, mica and platinum. *J. Am. Chem. Soc.* **1918**, *40*, 1361–1403. [[CrossRef](#)]
49. Halim, A.A.; Aziz, H.A.; Johari, M.A.M.; Ariffin, K.S. Comparison study of ammonia and COD adsorption on zeolite, activated carbon and composite materials in landfill leachate treatment. *Desalination*. **2010**, *262*, 31–35. [[CrossRef](#)]
50. Lagergren, S.Y.; Sven, K. Zurtheorie der sogenannten adsorption gelösterstoffe. *Kongliga Sven. Vetensk. Handl.* **1898**, *24*, 1–39.
51. Qiu, H.; Lv, L.; Pan, B.; Zhang, Q.; Zhang, W.; Zhang, Q. Critical review in adsorption kinetic models. *J. Zhejiang Univ. Sci. A* **2009**, *10*, 716–724. [[CrossRef](#)]
52. Ho, Y.S. Review of second-order models for adsorption systems. *J. Hazard. Mater.* **2006**, *136*, 681–689. [[CrossRef](#)] [[PubMed](#)]
53. Ho, Y.S.; McKay, G. A Comparison of chemisorption kinetic models applied to pollutant removal on various sorbents. *Process Saf. Environ. Prot.* **1998**, *76*, 332–340. [[CrossRef](#)]
54. Ho, Y.S.; McKay, G. Pseudo-second order model for sorption processes. *Process Biochem.* **1999**, *34*, 451–465. [[CrossRef](#)]
55. Dursun, G.; Çiçek, H.; Dursun, A.Y. Adsorption of phenol from aqueous solution by using carbonised beet pulp. *J. Hazard. Mater.* **2005**, *125*, 175–182. [[CrossRef](#)]
56. Mall, I.D.; Srivastava, V.C.; Agarwal, N.K. Removal of Orange-G and Methyl Violet dyes by adsorption onto bagasse fly ash—Kinetic study and equilibrium isotherm analyses. *Dye. Pigment.* **2006**, *69*, 210–223. [[CrossRef](#)]
57. Widiastuti, N.; Wu, H.; Ang, H.M.; Zhang, D. Removal of ammonium from greywater using natural zeolite. *Desalination* **2011**, *277*, 15–23. [[CrossRef](#)]
58. Boyd, G.E.; Adamson, A.W.; Myers, L.S. The Exchange Adsorption of Ions from Aqueous Solutions by Organic Zeolites. II. Kinetics. *J. Am. Chem. Soc.* **1947**, *69*, 2836–2848. [[CrossRef](#)]
59. Simonin, J.P.; Bouté, J. Intraparticle diffusion-adsorption model to describe liquid/solid adsorption kinetics. *Rev. Mex. Ing. Quim.* **2016**, *15*, 161–173.
60. Rudzinski, W.; Panczyk, T. Kinetics of isothermal adsorption on energetically heterogeneous solid surfaces: A new theoretical description based on the statistical rate theory of interfacial transport. *J. Phys. Chem. B* **2000**, *104*, 9149–9162. [[CrossRef](#)]
61. Cheung, C.W.; Porter, J.F.; McKay, G. Sorption kinetic analysis for the removal of cadmium ions from effluents using bone char. *Water Res.* **2001**, *35*, 605–612. [[CrossRef](#)]
62. Sağ, Y.; Aktay, Y. Kinetic studies on sorption of Cr(VI) and Cu(II) ions by chitin, chitosan and *Rhizopus arrhizus*. *Biochem. Eng. J.* **2002**, *12*, 143–153. [[CrossRef](#)]
63. Cortés-Martínez, R.; Martínez-Miranda, V.; Solache-Ríos, M.; García-Sosa, I. Evaluation of natural and surfactant-modified zeolites in the removal of cadmium from aqueous solutions. *Sep. Sci. Technol.* **2004**, *39*, 2711–2730. [[CrossRef](#)]
64. Wu, F.C.; Tseng, R.L.; Juang, R.S. Characteristics of Elovich equation used for the analysis of adsorption kinetics in dye-chitosan systems. *Chem. Eng. J.* **2009**, *150*, 366–373. [[CrossRef](#)]
65. Khan, A.A.; Singh, R.P. Adsorption thermodynamics of carbofuran on Sn (IV) arsenosilicate in H⁺, Na⁺ and Ca²⁺ forms. *Colloids Surf.* **1987**, *24*, 33–42. [[CrossRef](#)]
66. Giles, C.H.; MacEwan, T.H.; Nakhwa, S.N.; Smith, D. 786. Studies in adsorption. Part XI. A system of classification of solution adsorption isotherms, and its use in diagnosis of adsorption mechanisms and in measurement of specific surface areas of solids. *J. Chem. Soc.* **1960**. [[CrossRef](#)]
67. Dada, A.O. Langmuir, Freundlich, Temkin and Dubinin–Radushkevich Isotherms Studies of Equilibrium Sorption of Zn²⁺ onto Phosphoric Acid Modified Rice Husk. *IOSR J. Appl. Chem.* **2012**, *3*, 38–45. [[CrossRef](#)]
68. Alshameri, A.; Ibrahim, A.; Assabri, A.M.; Lei, X.; Wang, H.; Yan, C. The investigation into the ammonium removal performance of Yemeni natural zeolite: Modification, ion exchange mechanism, and thermodynamics. *Powder Technol.* **2014**, *258*, 20–31. [[CrossRef](#)]
69. Chabazite. Available online: <http://www.iza-online.org/natural/Datasheets/Chabazite/Chabazite.html> (accessed on 25 September 2020).
70. Ghosal, P.S.; Gupta, A.K. Determination of thermodynamic parameters from Langmuir isotherm constant-revisited. *J. Mol. Liq.* **2017**, *225*, 137–146. [[CrossRef](#)]

71. Xiang, L.; Wang, X.D.; Chen, X.H.; Mo, C.H.; Li, Y.W.; Li, H.; Cai, Q.Y.; Zhou, D.M.; Wong, M.H.; Li, Q.X. Sorption Mechanism, Kinetics, and Isotherms of Di- n-butyl Phthalate to Different Soil Particle-Size Fractions. *J. Agric. Food Chem.* **2019**, *67*, 4734–4745. [[CrossRef](#)] [[PubMed](#)]
72. Aydın Temel, F.; Kuleyin, A. Ammonium removal from landfill leachate using natural zeolite: Kinetic, equilibrium, and thermodynamic studies. *Desalin. Water Treat.* **2016**, *57*, 23873–23892. [[CrossRef](#)]

Publisher’s Note: MDPI stays neutral with regard to jurisdictional claims in published maps and institutional affiliations.



© 2020 by the authors. Licensee MDPI, Basel, Switzerland. This article is an open access article distributed under the terms and conditions of the Creative Commons Attribution (CC BY) license (<http://creativecommons.org/licenses/by/4.0/>).